Chemical Science

ROYAL SOCIETY OF CHEMISTRY

EDGE ARTICLE

View Article Online
View Journal | View Issue

Cite this: *Chem. Sci.*, 2024, **15**, 2243

All publication charges for this article have been paid for by the Royal Society of Chemistry

A living neutrophil Biorobot synergistically blocks multifaceted inflammatory pathways in macrophages to effectively neutralize cytokine storm†

Ya Gao,‡[a] Anwei Zhou,‡[b] Kerong Chen,[a] Xinyuan Zhou,[a] Yurui Xu,*[a] Shuangshuang Wu*[c] and Xinghai Ning *[a]

Received 5th July 2023
Accepted 20th December 2023

DOI: 10.1039/d3sc03438k

rsc.li/chemical-science

Cytokine storm is a potentially life-threatening immune response typically correlated with lung injury, particularly in people with underlying disease states, such as pneumonia. Therefore, the prompt treatment of cytokine storm is essential for successful recovery from a potentially fatal condition. Herein, a living anti-inflammatory Biorobot (firefighter), composed of neutrophils encapsulating mannose-decorated liposomes of the NF-κB inhibitor TPCA-1 and STING inhibitor H-151 (M-Lip@TH, inflammatory retardant), is developed for alleviating hyperinflammatory cytokine storm through targeting multiple inflammatory pathways in macrophages. Biorobot fully inherits the chemotaxis characteristics of neutrophils, and efficiently delivers and releases therapeutic M-Lip@TH at the inflammatory site. Subsequently, M-Lip@TH selectively targets macrophages and simultaneously blocks the transcription factor NF-κB pathway and STING pathway, thereby preventing the overproduction of cytokines. Animal studies show that Biorobot selectively targets LPS-induced acute lung injury, and not only inhibits the NF-κB pathway to suppress the release of various pro-inflammatory cytokines and chemokines, but also blocks the STING pathway to prevent an overactive immune response, which helps to neutralize cytokine storms. Particularly, Biorobot reduces lung inflammation and injury, improves lung function, and increases the survival rates of pneumonia mice. Therefore, Biorobot represents a rational combination therapy against cytokine storm, and may provide insights into the treatment of diseases involving overactive immune responses.

Introduction

Pneumonia is a potentially life-threatening medical condition that is caused by various pathogens, such as bacteria, viruses, fungi, or parasites.[1,2] Pneumonia is particularly dangerous for certain groups of people, such as young children, older adults, and those with weakened immune systems or underlying health conditions, and often leads to respiratory failure and other life-threatening complications.[3,4] For instance, severe COVID-19 pneumonia is often accompanied by a latent cytokine storm and related acute respiratory distress syndrome (ARDS), which may cause organ failure, shock, and even death.[5,6] Therefore, it is important to seek therapeutic approaches to calm cytokine storm and prevent complications in pneumonia, which is critical for reducing morbidity and mortality.

In recent years, great efforts have been made to explore immunomodulatory strategies to control pneumonia and associated syndromes, and diverse approaches to cytokine suppression have been developed, including the use of drugs that target specific cytokines as well as immunomodulatory therapies that regulate the immune system, which can help to manage inflammation, minimize tissue damage, and improve patient outcomes.[7,8] For example, the use of monoclonal antibodies has shown effectiveness in blocking the production or action of specific cytokines, such as interleukin-6 (IL-6) or tumor necrosis factor-alpha (TNF-α), which play significant roles in immune responses and inflammation. In addition, immunomodulatory therapies, such as corticosteroids or immunosuppressants, can help reduce the activity of immune

[a]*National Laboratory of Solid State Microstructures, Collaborative Innovation Center of Advanced Microstructures, Chemistry and Biomedicine Innovation Center, College of Engineering and Applied Sciences, Jiangsu Key Laboratory of Artificial Functional Materials, Nanjing University, Nanjing 210093, China. E-mail: xuyurui@nju.edu.cn; xning@nju.edu.cn*

[b]*National Laboratory of Solid State Microstructures, Collaborative Innovation Center of Advanced Microstructures, School of Physics, Nanjing University, Nanjing 210093, China*

[c]*Jiangsu Provincial Key Laboratory of Geriatrics, Department of Geriatrics, The First Affiliated Hospital with Nanjing Medical University, Nanjing 210029, China. E-mail: polariswu7632@njmu.edu.cn*

† Electronic supplementary information (ESI) available. See DOI: https://doi.org/10.1039/d3sc03438k

‡ These authors contributed equally to this work.

cells and consequently block the production of cytokines. Although these treatment strategies exhibit benefits in certain situations and have even demonstrated clinical efficacy in treating various inflammatory and autoimmune conditions, such as rheumatoid arthritis, psoriasis, bowel disease and especially pneumonia, most of them are designed to target single inflammatory pathways or specific cytokines. They may not always result in optimal treatment outcomes due to redundancy in inflammatory pathways, the heterogeneity of diseases, and resistance to therapy.[9–12] In particular, the immune system has multiple, overlapping pathways that can compensate for the inhibition of a single pathway. As a result, blocking one pathway may not be sufficient to control inflammation and immune responses in pneumonia. Additionally, non-targeted or non-specific immunotherapies often trigger unintended consequences or side effects in patients, resulting in severe restrictions.[13,14] Thus, the available clinical options for cytokine storm are limited, and continuing research and development of new therapies, as well as optimization of existing treatments, is constantly needed.[15]

It has been shown that immune cells play a critical role in initiating and perpetuating the inflammatory response. Once recruited, immune cells, such as neutrophils, macrophages, and T cells, release additional cytokines and other inflammatory mediators that amplify the inflammation. Therefore, controlling inflammatory cells is an important therapeutic goal to reduce cytokine storm symptoms, prevent tissue damage, and improve overall health outcomes.[16,17] In particular, macrophages have been proven to be critical for manipulating the progression of pulmonary inflammatory responses.[18] After infection and injury to the lungs, the toll-like receptors on macrophages recognize pathogen-associated molecular patterns (PAMPs), which are unique molecules found on the surface of pathogens such as viruses, bacteria, and fungi. This recognition triggers a signaling cascade within the macrophage, and consequently activates the transcription factor nuclear factor-kappa B (NF-κB), leading to the production and release of various cytokines and chemokines.[19] Additionally, the cyclic GMP-AMP synthase (cGAS) stimulator of interferon genes (STING) pathway in macrophages plays an important role in the innate immune response, particularly in the response to viral infections. The STING pathway can be activated by cytosolic DNA and triggers the expression of interferon (IFN), which consequently promotes the development of a cytokine storm.[20,21] Significantly, STING not only initiates but also modulates the NF-κB signaling pathway.[22] Concurrently, activation of NF-κB hinders STING degradation, which in turn enhances and prolongs the STING response. This interplay between NF-κB and STING orchestrates a cascade of amplified inflammatory responses and a robust immune defense. Thus, by concurrently inhibiting both the NF-κB and STING pathways, our strategy prevents compensatory activation within the NF-κB/STING signaling network, refines therapeutic dosing, and reduces administration frequency. This dual-pathway inhibition represents a powerful therapeutic approach to shield patients from severe cytokine storms and associated health complications. However, this type of study has been rarely reported so far.

In this study, for the first time, we have developed a living anti-inflammatory Biorobot (also referred to as a firefighter) to alleviate hyperinflammatory cytokine storm through simultaneously blocking the STING and NF-κB signaling pathways (Fig. 1). Biorobot is composed of living neutrophils encapsulating mannose-decorated liposomes of the NF-κB inhibitor TPCA-1 and STING inhibitor H-151 (M-Lip@TH), which act as inflammatory retardants. Recently, cell-based systems have been attracting increasing research attention,[23–26] and particularly, neutrophils as a major component of immunity in response to pathogen invasion, have been exploited as drug carriers to overcome multiple physiological barriers.[27,28] Importantly, neutrophils provide unique sustained release and specific delivery of drugs to inflammatory tissues, and have been applied in diverse applications.[29–31] In particular, neutrophils play a central role in the innate immune response to pathogens and tissue injury and can be recruited to inflamed lungs by chemokines and cytokines secreted by macrophages during pulmonary infection, suggesting that neutrophils are a promising carrier for targeting pneumonia.[32–34] Therefore, Biorobot might be able to not only target and migrate directly to the inflamed lungs, but also selectively release M-Lip@TH in response to inflammation, leading to good specificity for pneumonia. M-Lip@TH selectively targeted macrophages owing to mannose modification and enhanced intracellular transport of TPCA-1 and H-151, which could concurrently block multiple inflammatory pathways and significantly reduce cytokine storm syndromes, resulting in rapid recovery from pneumonia. The concurrent use of dual inhibitors demonstrates superiority over single-inhibitor therapies, synergistically suppressing the inflammatory pathways of NF-κB and STING, which results in reduced cytokine production. In conclusion, this medication has the potential to manage various inflammatory and autoimmune conditions by modulating the immune response, reducing inflammation, and preventing tissue damage, which may provide insight into the development of anti-inflammatory treatment approaches.

Results and discussion

Preparation and characterization of Biorobot

In pneumonia, macrophages are recruited to the infected lungs to defend against invading pathogens, such as bacteria, viruses, and fungi. Importantly, macrophages release cytokines, as well as activating and coordinating the immune response to infections. However, an uncontrolled inflammatory response may lead to high immunopathology and mortality.[35,36] To alleviate hyperinflammatory cytokine storm, we developed a smart Biorobot, which was composed of mannose-decorated liposomes (M-Lip@TH) loaded in neutrophils. To construct Biorobot, M-Lip@TH was first prepared by encapsulating a STING inhibitor (H-151) and IKK inhibitor (TPCA-1) in mannose-modified liposomes using a thin lipid film hydration method, generating uniform nanoparticles with a mean size of 112.35 ± 0.38 nm and zeta potential of −17.21 ± 1.48 mV (Fig. 2A and B).

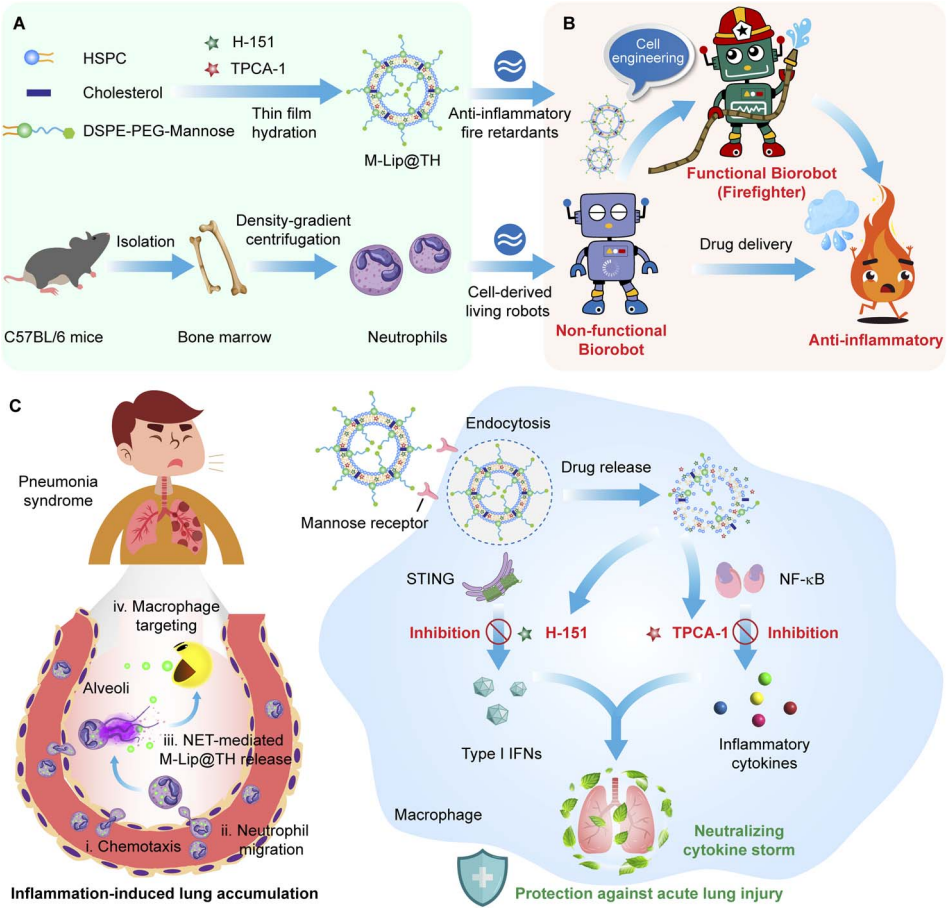

Fig. 1 A living anti-inflammatory Biorobot effectively neutralizes cytokine storm through synergistically blocking multiple inflammatory pathways in macrophages. (A) Schematic illustration of the preparation of Biorobot. Mature neutrophils are isolated from mouse bone marrow then purified using density-gradient centrifugation. In addition, a mannose-decorated liposomal formulation of the NF-κB inhibitor TPCA-1 and STING inhibitor H-151 (M-Lip@TH) is prepared using a thin lipid film hydration method. Next, Biorobot is constructed by encapsulating M-Lip@MH inside the neutrophils. (B) Visual depiction of the biological engineering of Biorobot. Due to their unique characteristics, neutrophils are a potential drug carrier. The idea is to take advantage of their natural ability to migrate to inflammatory sites and deliver drugs directly to these areas. This approach can help to increase the effectiveness of drugs and reduce side effects. Specifically, neutrophils can act as a Biorobot with inflammation-targeting ability, which can be further functionalized by encapsulating inflammatory retardant M-Lip@TH, generating the functional Biorobot (firefighter). Importantly, the functional Biorobot can simultaneously alleviate the over-activation of the NF-κB and STING pathways in pneumonia, resulting in the rapid relief of cytokine storm. (C) Therapeutic mechanism of Biorobot for treating cytokine storm. Biorobot fully inherits the chemotaxis characteristics of neutrophils and can efficiently deliver and release M-Lip@TH at inflammatory sites. Subsequently, M-Lip@TH not only improves macrophage uptake, but effectively inhibits the STING and NF-κB signaling pathways involved in the immune response, thereby preventing the emergence of cytokine storm and achieving desirable therapeutic outcomes.

Next, we evaluated the drug loading (DL) rate and encapsulation efficiency (EE) of H-151 and TPCA-1 in M-Lip@TH. Table S1† shows that the DL and EE of H-151 were 2.46 ± 0.12% and 98.40 ± 0.26%, respectively, and the DL and EE of TPCA-1 were 2.47 ± 0.11% and 98.90 ± 0.19%, suggesting that H-151 and TPCA-1 were effectively encapsulated in M-Lip@TH. In addition, we also investigated the stability of M-Lip@TH. As shown in Fig. 2C and D, no changes in the size or zeta potential of M-Lip@TH were observed after 14 days of incubation in PBS at 4 °C, or after 24 h of incubation in 50% fetal bovine serum at 37 °C, respectively. Importantly, only about 14% of the TPCA-1 and 11% of the H-151 were released from M-Lip@TH within 24 h (Fig. 2E). These data suggest that M-Lip@TH has good stability, which is beneficial for the subsequent construction of Biorobot.

Next, neutrophils were isolated from mouse bone marrow and purified to a 92% purity level *via* density-gradient centrifugation, as presented in Fig. S1.† This high degree of purity is advantageous for the subsequent construction of our Biorobot, and they can be used for various downstream applications, such as study of their function or use in *in vitro* or *in vivo* experiments. Moreover, Biorobot was prepared by incubating neutrophils with M-Lip@TH. To validate the successful encapsulation of M-Lip@TH within live neutrophils, we conducted a sodium dodecyl sulfate-polyacrylamide gel electrophoresis (SDS-PAGE) assay. This analysis was aimed at detecting the complete spectrum of neutrophil membrane and cellular proteins within Biorobot. The results, which are depicted in Fig. S2,† confirm the presence of the full complement of

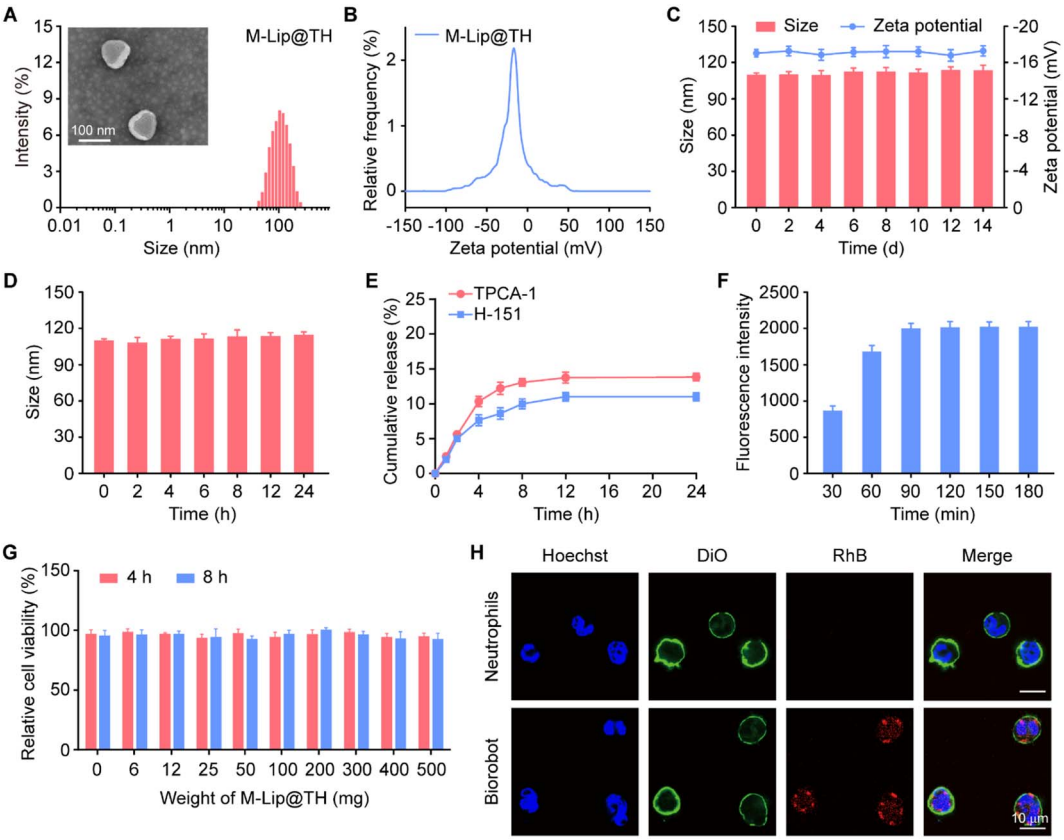

Fig. 2 Preparation and characterization of Biorobot. (A) DLS data of M-Lip@TH. (Upper inset) TEM image of M-Lip@TH. Scale bar: 100 nm. (B) Zeta potential of M-Lip@TH. (C) Physical stability of M-Lip@TH in PBS at 4 °C over 14 days. (D) Serum stability of M-Lip@TH at 37 °C over 24 h. (E) Time-dependent release of TPCA-1 and H-151 from M-Lip@TH in PBS over 24 h. (F) Cellular uptake of RhB-labeled M-Lip@TH in neutrophils over 180 min. (G) Biosafety of M-Lip@TH in neutrophils after 4 h or 8 h of incubation. (H) Confocal images of neutrophils and RhB-labeled M-Lip@TH-treated neutrophils. Scale bar: 10 μm. The data are presented as mean ± s.d. ($n = 6$).

neutrophil proteins in Biorobot. This finding strongly indicates that M-Lip@TH has been successfully incorporated into the neutrophils, endowing them with inherent motility and the ability to chemotactically navigate toward inflamed lung tissue. The cellular uptake and cytotoxicity of M-Lip@TH in neutrophils were then investigated; RhB-labeled M-Lip@TH was incubated with neutrophils for 180 min, and the intracellular fluorescence signals were monitored using flow cytometry. As shown in Fig. 2F, strong fluorescence was observed in the neutrophils, indicating that M-Lip@TH can be efficiently taken up by the neutrophils. Additionally, we identified that M-Lip@TH had negligible cytotoxicity towards neutrophils at all the studied concentrations from 6 to 500 mg mL^{-1} after 8 h of treatment (Fig. 2G). Low cytotoxicity toward neutrophils is an important characteristic for M-Lip@TH that are intended to be used in or on the body, as it ensures that they do not harm the immune system and can be safely used without causing harmful side effects. In addition, the loading capacity of Biorobot in neutrophils was also evaluated, generating a loading rate of 5.9 μg H-151 and 5.93 μg TPCA-1 per 10^6 cells (Fig. S3†), respectively, suggesting that an adequate amount of the therapeutic agent to achieve the desired therapeutic effect was incorporated into Biorobot. This is important for ensuring the efficacy of the drug and minimizing potential side effects. Importantly, no morphological changes in the neutrophils were observed after the encapsulation of M-Lip@TH, which was confirmed by confocal laser scanning microscopy (CLSM) and Giemsa–Wright staining (Fig. 2H and Fig. S4†). Morphological changes in neutrophils can be an important indicator of various health conditions, and the absence of morphological changes means that the neutrophils are healthy.

Biological characterization of Biorobot

Neutrophils are crucial for immune defense, and understanding their physiological functions is essential for developing therapeutic strategies to modulate their activity in various disease conditions. We therefore evaluated the physiological functions of Biorobot, including CD11b protein expression and cell migration behavior. It has been shown that neutrophil migration is a multistep process that involves several distinct stages. This process is critical for the recruitment of neutrophils to sites of infection or inflammation, where they can help to eliminate invading pathogens. In particular, proteins that trigger cell adhesion and detachment play a key role in neutrophil migration.[37] For instance, CD11b, also known as integrin alpha M, is a cell surface protein expressed on

neutrophils, and plays a crucial role in the immune response, particularly in cell adhesion, migration, and phagocytosis, which are essential for the proper functioning of neutrophils during an immune response.[38,39] Next, we investigated and compared the expression levels of CD11b on blank neutrophils and Biorobot under the stimulation of *N*-formyl-methionyl-leucyl-phenylalanine (fMLP). fMLP is a potent chemoattractant peptide that can stimulate various immune cells to migrate towards the source of the stimulus. When neutrophils are exposed to fMLP, they undergo a series of signaling events that ultimately lead to the upregulation of CD11b expression on their surface. Fig. 3A shows that the blank neutrophils and Biorobot exhibited a similar increase in inflammatory markers in response to fMLP, and the levels of CD11b increased with increasing concentrations of fMLP. This increase in CD11b expression is an important mechanism by which neutrophils respond to chemotactic stimuli, suggesting that the encapsulation of M-Lip@TH has minimal effects on neutrophils. Moreover, we also tested the chemotaxis activity of Biorobot using a transwell migration assay. Neutrophils have the ability to migrate towards sites of infection or inflammation in response to various chemical signals, including chemokines, cytokines, and bacterial products, allowing neutrophils to quickly reach sites of inflammation. As shown in Fig. 3B, Biorobot could migrate to the lower chamber of a transwell in the presence of fMLP and exhibited similar migration capability to neutrophils. Taken together, these data confirm that Biorobot has inflammation-targeting capability, which might help to control inflammation and improve outcomes in various inflammatory and infectious diseases.

Furthermore, we explored the stability of M-Lip@TH in neutrophils using the fluorescence resonance energy transfer (FRET) assay, which is a valuable tool for studying molecular interactions at the nanometer scale. FRET is based on the non-radiative transfer of energy between two fluorophores, a donor and an acceptor, when they are in close proximity (typically within 10 nm). In this study, DiO and DiI were used as the donor and acceptor, respectively, to construct liposomes (DiO/DiI-M-Lip@TH) in which DiO generated green fluorescence (510 nm) under 480 nm excitation, which could transfer to DiI, resulting in red fluorescence (585 nm) (Fig. 3C). Fig. 3D shows that DiO/DiI labeled M-Lip@TH in neutrophils maintained the FRET effect under normal physiological conditions for 4 h. Similarly, strong red fluorescence from DiO/DiI-M-Lip@TH was observed in Biorobot after 4 h of incubation, as observed using CLSM (Fig. 3E), confirming the good stability of M-Lip@TH in neutrophils. In addition, we measured the inflammation-triggered drug release profiles of Biorobot, in which Biorobot was treated with phorbol myristate acetate (PMA), a chemical compound that is commonly used in scientific research to activate protein kinase C (PKC) in cells. When neutrophils are exposed to PMA, it activates PKC, which in turn triggers a signaling cascade that leads to the production of reactive oxygen species (ROS) and the release of DNA and other neutrophil extracellular trap (NET) components. This process is known as NETosis, and plays an important role in the immune response to bacterial and fungal infections. After treatment with PMA, the extracellular fluorescence signals from Biorobot were measured. As shown in Fig. S5,† efficient FRET was observed in the supernatant of PMA-treated Biorobot under the excitation of

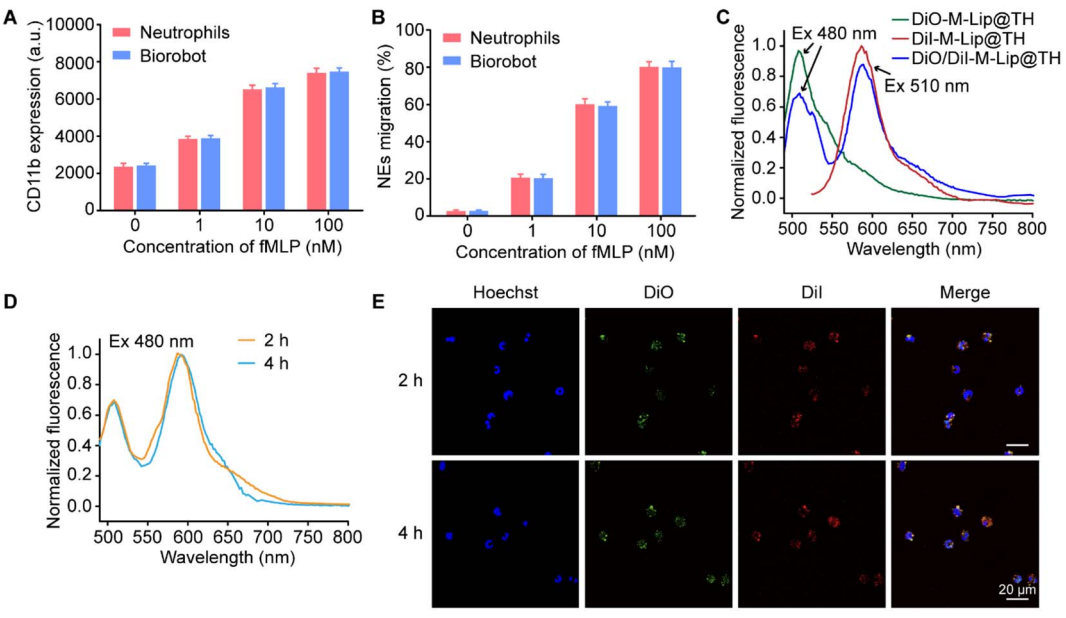

Fig. 3 Biological characteristics of Biorobot. (A) Expression of CD11b on Biorobot in response to fMLP. (B) Migration of neutrophils and Biorobot after incubation with different concentrations of fMLP. (C) Emission spectra of DiO-labeled M-Lip@TH, DiI-labeled M-Lip@TH and DiO/DiI-labeled M-Lip@TH under different excitation wavelengths. (D) Identification of the integrity of DiO/DiI-labeled M-Lip@TH in neutrophils through the FRET effect. (E) Confocal images of neutrophils after incubation with DiO/DiI-labeled M-Lip@TH for 2 h and 4 h. Scale bar: 20 μm. The data are presented as mean ± s.d. ($n = 6$).

480 nm light. In contrast, untreated Biorobot exhibited minimal fluorescence signals in the supernatant, suggesting that M-Lip@TH maintains its integrity in neutrophils, but can be released under inflammatory stimuli. Therefore, Biorobot exhibits potent therapeutic potential for the management of inflammatory diseases.

Biorobot-mediated selective delivery of M-Lip@TH in macrophages

Targeted delivery of therapeutic agents specifically to macrophages can improve the efficacy of therapies by ensuring that the drugs are delivered directly to the site of the disease. This targeted approach can increase the concentration of the drug at the site of action, leading to more effective treatment with fewer side effects. One way to achieve selective delivery of therapeutic agents to macrophages is through the use of liposomes, which can be designed to be functionalized with ligands that specifically bind to macrophage surface receptors, such as the mannose receptor or the scavenger receptor. Once these nanoparticles are internalized by macrophages, they can release their cargo directly into the cells, thereby achieving targeted drug delivery. We therefore evaluated the capability of Biorobot to selectively deliver drugs in macrophages. Specifically, the inflammation-stimulated release of M-Lip@TH from Biorobot and subsequent cellular uptake of M-Lip@TH in macrophages were measured. Fig. 4A shows that M-Lip@TH was rapidly released from Biorobot in the presence of PMA, whereas negligible M-Lip@TH release was observed from untreated Biorobot, indicating the responsive characteristics of Biorobot, which enable it to release a substance or payload in response to inflammatory stimuli.

In addition, we evaluated whether mannose decoration could improve the cellular uptake of M-Lip@TH in RAW 264.7 cells. The mannose receptor is a type of receptor found on the surface of macrophages, and targeting the mannose receptor can be used a strategy to enhance the delivery of drugs or toxins directly to macrophages. Fig. S6† shows that M-Lip@TH rapidly accumulated in RAW 264.7 cells, generating 1.59-fold higher fluorescence intensity than Lip@TH without mannose modification, which could improve the effectiveness of treatments. Next, we investigated the ability of Biorobot to enhance the delivery of drugs to macrophages, in which Biorobot was co-cultured with RAW 264.7 cells for 24 h in the presence of PMA, followed by measuring the cell uptake of M-Lip@TH in RAW 264.7 cells by flow cytometry. As shown in Fig. 4B, the cellular uptake of the released M-Lip@TH in RAW 264.7 cells gradually increased in a time-dependent manner, and reached a plateau within 12 h. Additionally, the uptake of the released M-Lip@TH in RAW 264.7 cells was also explored using CLSM (Fig. 4C). Low levels of M-Lip@TH were detected in RAW 264.7 cells after co-culturing with Biorobot in the absence of PMA. These data suggest that Biorobot not only achieves the inflammation-triggered release of encapsulated M-Lip@TH, but effectively targets macrophages to improve the treatment outcomes.

In addition to active transport, the release of drugs from nanoparticles after cell uptake is a crucial step in achieving effective intracellular drug delivery. Nanoparticles can be engineered with various properties and materials to facilitate drug release. For instance, the use of liposomes as drug delivery vehicles can improve the release of the encapsulated drug through fusion of the liposome membrane with the cellular membrane, making them promising drug delivery vehicles. We next investigated the degradation of M-Lip@TH in RAW 264.7 cells using a FRET assay in which RAW 264.7 cells were incubated with DiO/DiI-M-Lip@TH, followed by monitoring FRET effects during culture. As shown in Fig. 4D, upon excitation at 480 nm, the red fluorescence of DiI gradually decreased with increasing culture duration, whereas the green fluorescence of DiO increased with culture time. Additionally, an attenuated FRET effect in RAW 264.7 cells was also identified using a fluorescence spectrofluorometer (Fig. 4E), which indicated the disassembly of M-Lip@TH in RAW 264.7 cells, which would allow the release of the therapeutic agents directly into the cells. Importantly, we identified that M-Lip@TH exhibited no apparent cytotoxicity toward macrophages and did not cause cell death or damage (Fig. 4F), suggesting that M-Lip@TH may be safe for use in relation to these cells. Therefore, M-Lip@TH has the appropriate physicochemical properties, targeting mechanisms, and intracellular drug release, and may improve the pharmacokinetic and pharmacodynamic properties of drugs, which is beneficial for *in vivo* applications.

In vitro anti-inflammatory effects of Biorobot

Moreover, we investigated the anti-inflammatory activity of Biorobot against the secretion of pro-inflammatory cytokines in macrophages. Macrophages are major immune cells and play an important role in the innate immune response, which is the body's first line of defence against invading pathogens and other harmful organisms.[40] Upon recognition of pathogen-associated molecular patterns (PAMPs), macrophages are activated to initiate inflammation through the release of cytokines (Fig. 5A).[41] For example, lipopolysaccharide (LPS), a major endotoxin found in the outer membrane of Gram-negative bacteria, plays a crucial role in the activation of the innate immune response. When LPS is recognized by toll-like receptor 4 (TLR4) on the surface of macrophages and other immune cells, it triggers a cascade of intracellular signaling events that ultimately activate the NF-κB and interferon regulatory factor 3 (IRF3) pathways, leading to the production of pro-inflammatory cytokines and interferons. In addition, polyinosinic–polycytidylic acid [poly(I:C)] is a synthetic double-stranded RNA (dsRNA) that mimics the structure of viral dsRNA found in some viruses. When present in the cellular environment, poly(I:C) is recognized by Toll-like receptor 3 (TLR3), which is expressed in macrophages, leading to the activation of the NF-κB and IRF3 signaling pathways, which ultimately trigger the production of inflammatory cytokines.[42] Moreover, aberrant cytosolic double-stranded DNA (dsDNA), which can arise from viral infections, bacterial infections, or cellular damage, is recognized by the cGAS enzyme. This recognition leads to the activation of the STING pathway, which in turn activates both IRF3-dependent and NF-κB-dependent signaling transduction pathways. This

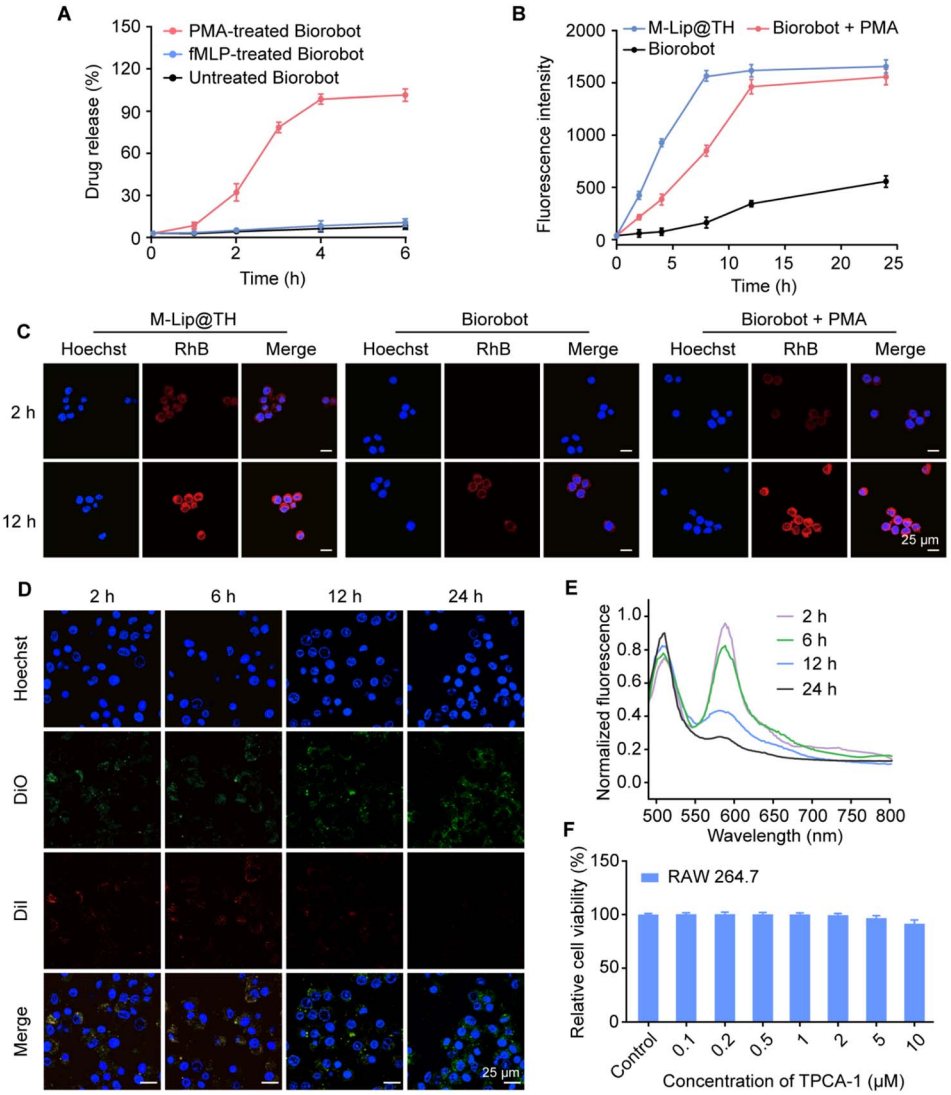

Fig. 4 Biorobot-mediated selective delivery of M-Lip@TH in macrophages. (A) Inflammation-triggered drug release profile of Biorobot. Biorobot was incubated with PMA (100 nM) for 6 h, followed by measurement of the time-dependent release of M-Lip@TH. (B) Biorobot-mediated selective uptake of M-Lip@TH in macrophages. RAW 264.7 cells were cultured with RhB-labeled Biorobot in the presence of PMA for 24 h, followed by measurement of intracellular fluorescence signals using flow cytometry. (C) Confocal images of RAW 264.7 cells after incubation with RhB-labeled M-Lip@TH, and RhB-labeled Biorobot with or without PMA for 2 h and 12 h. Scale bar: 25 μm. (D) Confocal images of DiO/DiI-labeled M-Lip@TH in macrophages at different time points. Scale bar: 25 μm. (E) Identification the integrity of M-Lip@TH in Biorobot. The emission spectra of DiO/DiI-labeled M-Lip@TH in Biorobot were monitored under the excitation wavelength of 480 nm at different time points. (F) Cell viability of RAW 264.7 cells after treatment with Biorobot in the presence of PMA. Data are presented as mean ± s.d. ($n = 6$).

ultimately results in the regulation of the transcription of inflammatory cytokines, which are essential components of the innate immune response.[43] Therefore, macrophage-associated inflammatory pathways provide a good therapeutic target for modulating inflammation.[44,45]

In this study, we developed a dual-inhibitor system composed of NF-κB inhibitor TPCA-1 and STING inhibitor H-151 for inhibiting the production of inflammatory cytokines in macrophages. To examine its anti-inflammatory effects, RAW 264.7 cells were pretreated with LPS, poly(I:C) or dsDNA for 6 h, followed by incubation with Biorobot (containing 1 μM TPCA-1 and 1 μM H-151) in the presence of PMA (100 nM) for 24 h. The extracellular levels of inflammatory cytokines and nitrite were measured using enzyme-linked immunosorbent assay (ELISA). As expected, in comparison to the control, LPS, poly(I:C) and dsDNA caused greater activation of RAW 264.7 cells and improved the production of inflammatory cytokines, including TNF-α, IL-6, monocyte chemotactic protein 1 (MCP-1) and interferon-β (IFN-β), as well as nitric oxide (NO) (Fig. 5B–F). Importantly, treatment with Biorobot significantly reduced the production of inflammatory cytokines, indicating the synergistic anti-inflammatory effect of TPCA-1 and H-151.

Furthermore, it has been reported that, in addition to direct pathogen invasion, cellular stress or damage caused by infections and inflammation can lead to the release of dsDNA into the cytoplasm, which can also be recognized by the cGAS-STING

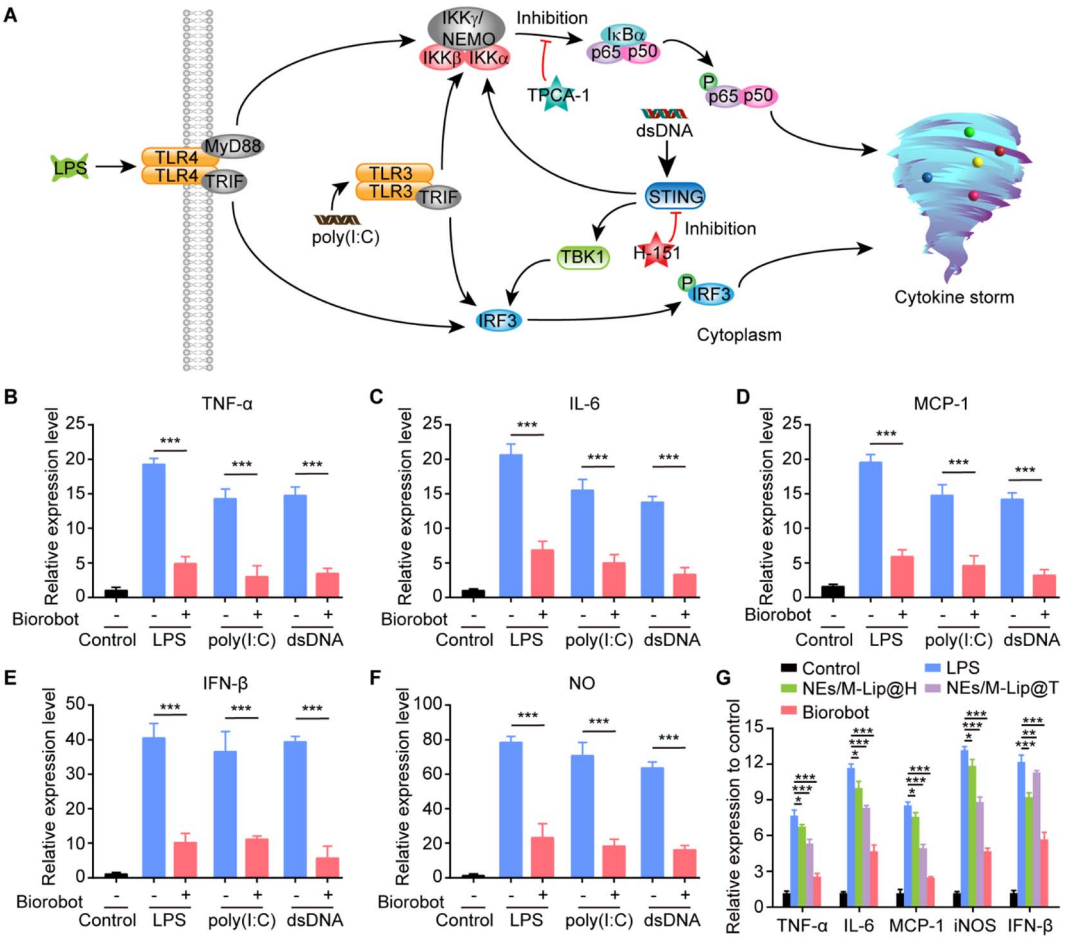

Fig. 5 *In vitro* anti-inflammatory effects of Biorobot. (A) Schematic representation of the inhibitory effects of Biorobot on the LPS-TLR4, poly(I:C)-TLR3, and dsDNA-STING signaling pathways. (B–F) Inhibition activity of Biorobot against the production of TNF-α induced by LPS, poly(I:C) and dsDNA (B), IL-6 (C), MCP-1 (D), IFN-β (E), and NO (F). RAW 264.7 cells were pretreated with LPS, poly(I:C) or dsDNA for 6 h, followed by incubation with Biorobot in the presence of PMA for 24 h. The production of different inflammatory cytokines and chemokines was measured. (G) Inhibitory effects of different agents on the gene expression of inflammatory cytokines in macrophages under the stimulation of LPS. The data are presented as mean ± s.d. ($n = 6$). * represents $p < 0.05$. ** represents $p < 0.01$. *** represents $p < 0.001$.

pathway and leads to inflammatory disease.[46] We therefore investigated whether Biorobot could ameliorate LPS-induced inflammation; for this, RAW 264.7 cells were pretreated with LPS for 6 h and then treated with Biorobot in the presence of PMA (100 nM) for 24 h, followed by measurement the gene expression of different inflammatory factors. This study provides insight into the molecular mechanisms underlying inflammation and may lead to the identification of new targets for therapeutic interventions. As shown in Fig. 5G, in comparison to the single inhibition groups containing TPCA-1 or H-151, Biorobot-treated group inhibited the expression of inflammation genes, and the genes responsible for triggering an inflammatory response were not highly active or expressed. We conducted further evaluations of the regulatory effects of Biorobot on the STING and NF-κB signaling pathways in macrophages through western blot analysis. The results, which are depicted in Fig. S9,† demonstrate minimal phosphorylation of the NF-κB subunit p65 and TBK1 proteins following treatment with Biorobot, indicating the targeted modulation of these signaling pathways. Collectively, this evidence substantiates the selective inhibition of both NF-κB and STING pathways by Biorobot, underpinning its anti-inflammatory capabilities. Taken together, Biorobot provides a promising platform that can have a synergistic effect with high anti-inflammation potency.

In vivo inflammation targeting of Biorobot in pneumonia mice

Based on the *in vitro* studies, we investigated the inflammation targetability and therapeutic efficacy of Biorobot in mice with LPS-induced pneumonia, which is a common model used in laboratory studies to simulate bacterial pneumonia in humans. Inflammation can create a variety of barriers that make it difficult for drugs to reach their intended target site, which can limit their effectiveness. One of the major barriers is the increased permeability of blood vessels in inflamed tissue, which can cause drugs to leak out of the blood vessels and into the surrounding tissue, reducing their concentration at the

target site. To overcome these passive targeting barriers, we developed a neutrophil-based drug carrier to encapsulate drugs and protect them from degradation or sequestration, which could potentially improve the efficacy of drugs for treating inflammation. Therefore, we first investigated the ability of Biorobot to selectively accumulate at inflammatory sites. Healthy mice or LPS-induced pneumonia mice were intravenously administered DiR-labeled M-Lip@TH (DiR-M-Lip@TH) or DiR-labeled Biorobot (DiR-Biorobot), followed by imaging with an IVIS imaging system for 24 h. Fig. 6A shows that DiR-M-Lip@TH accumulated in the liver of healthy and pneumonia mice within 4 h. In contrast, DiR-Biorobot selectively accumulated in lung tissues and generated much higher fluorescence signals in lungs with pneumonia than those in healthy mice (Fig. 6B). In addition, the major organs were harvested and imaged after 24 h administration. As shown in Fig. 6C, DiR-M-Lip@TH mainly accumulated in the liver and spleen in both healthy and pneumonia mice. However, in addition to targeting the liver and spleen of healthy mice, DiR-Biorobot also accumulated in lung tissues. Importantly, much higher accumulation of DiR-Biorobot in the lungs was observed in pneumonia mice, compared with that in the liver and spleen. Tissue distribution results were consistent with previous reports about the ability of neutrophils to migrate towards inflammatory tissues, which is a critical component of the immune response against inflammation. Furthermore, the lung tissues were frozen, sliced, and stained with DAPI for histological analysis. DAPI is a fluorescent stain that binds to DNA, allowing for visualization of nuclei within the tissue sections, which can provide information about the cellular composition and organization of the lung tissue, as well as potential abnormalities such as inflammation. As shown in Fig. 6D, the red fluorescence of the DiR-Biorobot-treated lung was higher than that of DiR-M-Lip@TH-treated group. Taken together, these data suggest that Biorobot can retain the function of neutrophils and is indeed capable of targeting a specific region, *i.e.*, the lung with pneumonia.

In vivo anti-inflammatory effects of Biorobot in LPS-induced pneumonia mice

Finally, we investigated the *in vivo* anti-inflammatory effects of Biorobot in an acute pneumonia model, which was established by intranasal administration of LPS (4 mg kg^{-1}). Next, pneumonia mice were intravenously administered phosphate buffer saline (PBS) or Biorobot (1 mg kg^{-1} TPCA-1 and 1 mg kg^{-1} H-151). The lung bronchoalveolar lavage fluid (BALF) were collected at 0 h, 12 h, 24 h, 48 h and 72 h after administration (Fig. 7A). The healthy mice served as the control. As previously reported, inflammatory proteins, such as cytokines, are released by the immune system in response to an infection or injury and play an important role in fighting off the invading pathogen. However, in some cases, the immune response can become overactive and lead to a phenomenon known as a cytokine storm, which can cause damage to healthy tissues in the body and even death.[47] Therefore, we first evaluated the cytokine levels in acute pneumonia mice after treatment with Biorobot. As shown in Fig. 7B–F, in comparison to the PBS-treated group, Biorobot effectively reduced the production of inflammatory cytokines and NO in the lung tissues, indicating that Biorobot may prevent the emergence of cytokine storms *in vivo*.

In addition, it has been shown that acute pneumonia can lead to several changes in lung tissue, including increased thickness of the alveolar layer, infiltration of immune cells into

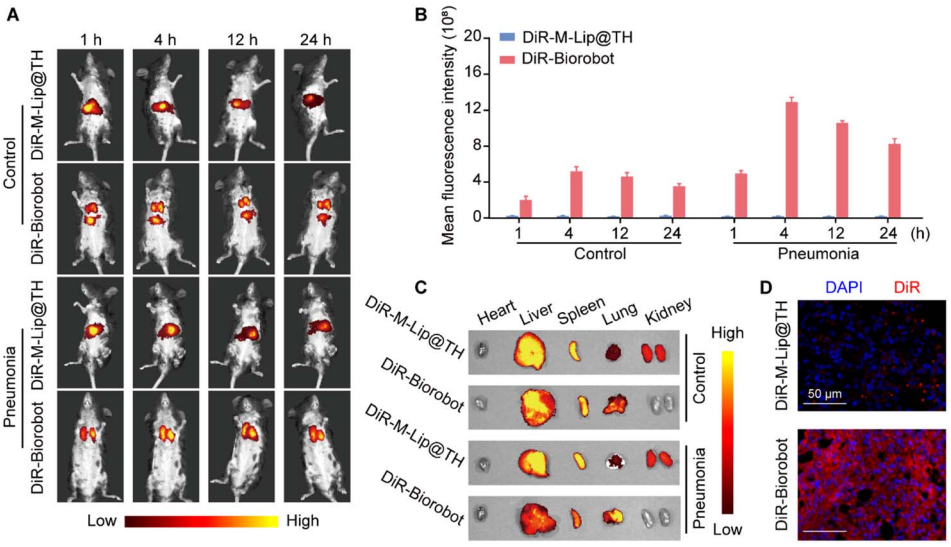

Fig. 6 *In vivo* inflammation targeting of Biorobot in pneumonia mice. (A) Time-dependent *in vivo* fluorescence imaging of pneumonia mice after intravenous injection of DiR-labeled M-Lip@TH or neutrophils. Both healthy and pneumonia mice were intravenously injected with DiR-M-Lip@TH or DiR-Biorobot and imaged with an IVIS imaging system for 24 h. (B) Mean fluorescence intensity of the lung regions at different time points after the intravenous injection of DiR-M-Lip@TH or DiR-Biorobot. (C) *Ex vivo* fluorescence images of major organs after 24 h treatment of DiR-M-Lip@TH or DiR-Biorobot. (D) Confocal images of lung sections treated with DiR-M-Lip@TH or DiR-Biorobot. Scale bar: 50 μm. The data are presented as mean ± s.d. ($n = 6$).

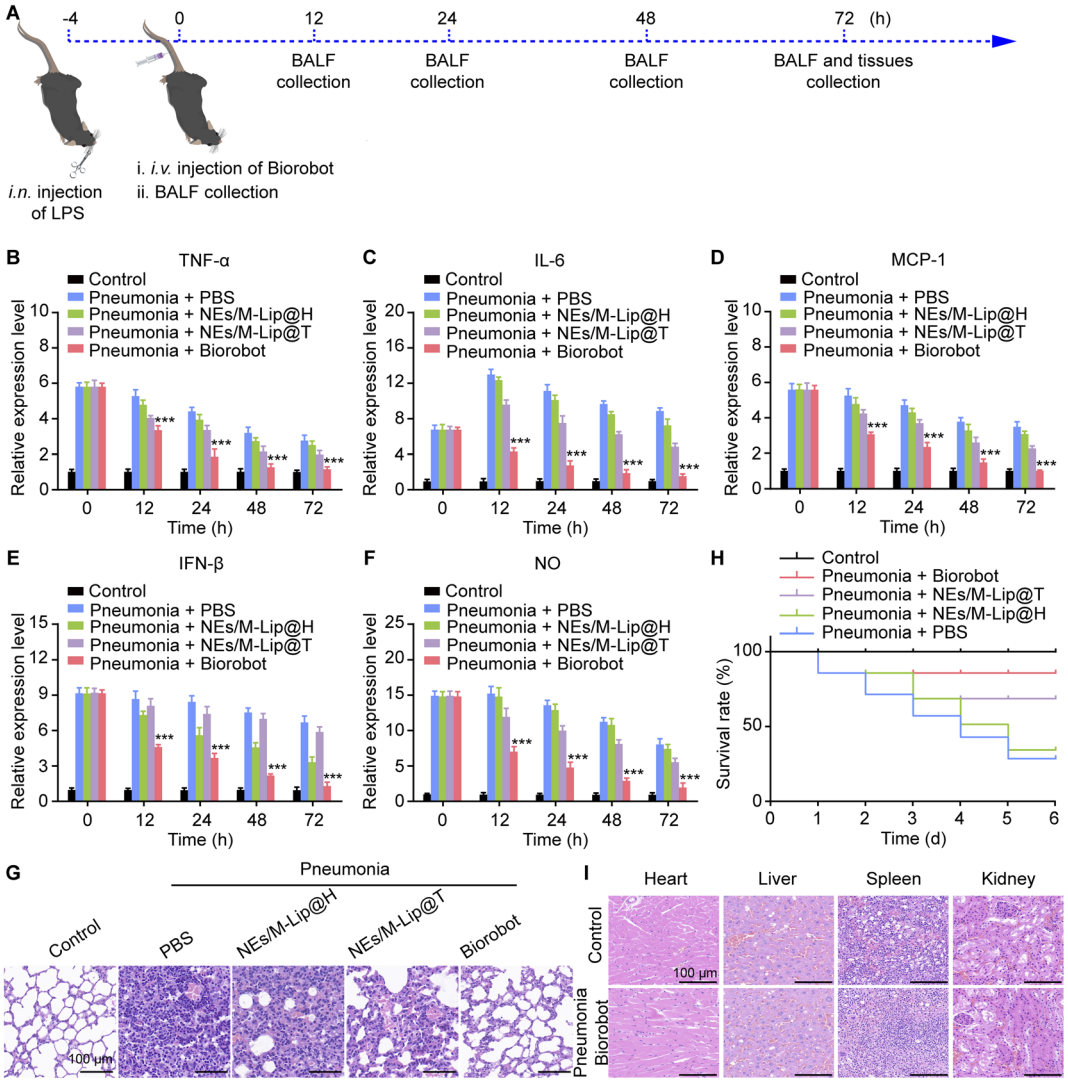

Fig. 7 *In vivo* anti-inflammatory effects of Biorobot in LPS-induced pneumonia mice. (A) Scheme of therapeutic plan for the treatment of pneumonia mice. (B–F) Time-dependent production of TNF-α (B), IL-6 (C), MCP-1 (D), IFN-β (E), and NO (F) in BALF of pneumonia mice during the treatment. (G) Hematoxylin–eosin staining of the lungs of healthy mice and pneumonia mice after the treatment. Scale bar: 100 μm. (H) Survival curves of pneumonia mice after the treatment. (I) Hematoxylin–eosin staining of major organs in healthy mice and pneumonia mice after the treatment. Scale bar: 100 μm. The data are presented as mean ± s.d. ($n = 6$). *** represents $p < 0.001$.

the lung tissue, and destruction of the alveolar septa. We therefore performed a histological examination and validated the existence of excessive pulmonary edema, alveolar inflammatory cell infiltration, and alveolar injury in the PBS-treated group. However, Biorobot treatment significantly reduced acute lung injury and respiratory distress syndrome (Fig. 7G), indicating that Biorobot can reach the inflamed lung and achieve the desired therapeutic effects. Moreover, Biorobot demonstrated a reduction in the proportion of M1 macrophages within the lung tissues compared to the untreated pneumonia group, as depicted in Fig. S10.† This finding suggests that Biorobot can modulate M1 macrophage activity by concurrently inhibiting the STING and NF-κB signaling pathways. Importantly, Biorobot intervention resulted in an increase in the survival rate of mice with acute pneumonia (Fig. 7H). Moreover, further analysis revealed that Biorobot possesses favorable biocompatibility. Hematoxylin–eosin staining affirmed the absence of any tissue damage attributable to Biorobot in critical organs including the heart, liver, spleen, and kidney, as depicted in Fig. 7I. This finding was substantiated by the consistent hematological indices (Fig. S11†), indicating no adverse systemic effects. Collectively, these observations support the viability of Biorobot-based dual inhibitor therapy as an innovative and promising approach for the effective management of inflammatory diseases, with the potential to confer multiple therapeutic advantages.

In vivo transcriptomic profiling of Biorobot-treated pneumonia mice

To gain a deeper understanding of the mechanism underlying the treatment using Biorobot against cytokine storm,

a transcriptomics analysis was performed on the lung tissues of the LPS-induced pneumonia mice after treatment. Transcriptomics is the study of the complete set of RNA transcripts produced by the genome under specific conditions, which can provide insights into the gene expression patterns and molecular pathways associated with the immune response to LPS and the subsequent treatment. Firstly, we identified that 13 978 genes were co-expressed in both groups, 647 genes were exclusively expressed in the PBS group and 1571 genes were only expressed in the Biorobot group (Fig. 8A). Moreover, a gene expression analysis identified 2781 genes that were differentially expressed between the two groups. Out of these, 1284 genes were found to be upregulated (*i.e.*, expressed at higher levels) in one group compared to the other, while 1497 genes were found to be downregulated (*i.e.*, expressed at lower levels) in the same comparison (Fig. 8B). This study determined the changes in gene expression in the mice before and after treatment with Biorobot, which may provide insight into the potential mechanism of action of Biorobot.

Moreover, to elucidate the therapeutic mechanism of Biorobot, we performed Gene Ontology (GO) enrichment analysis to analyze the differentially expressed genes between two groups. The purpose of this analysis is to identify GO terms, which are functional annotations assigned to genes based on their treatment outcomes. As shown in Fig. 8C, 2781 genes were found to be differentially regulated in the Biorobot group. Based on the GO analysis, it appears that these genes are mainly associated with various aspects of the immune response, including immunoglobulin-mediated immune response, macrophage activation, chemokine-mediated signaling pathway, leukocyte activation involved in inflammatory response, regulation of cytokine production involved in immune response, and cytokine secretion. This information suggests that Biorobot group may have an altered immune response compared to the control group. In particular, the GO enrichment chord diagram (Fig. 8D) shows that the top 10 significantly enriched GO terms are related to inflammatory responses and cytokine signaling pathways. All in all, Biorobots can downregulate several inflammatory-related pathways compared with a control group, which suggests that the synergistic inhibition effects of TPCA-1 and H-151 can effectively ameliorate cytokine storm syndromes.

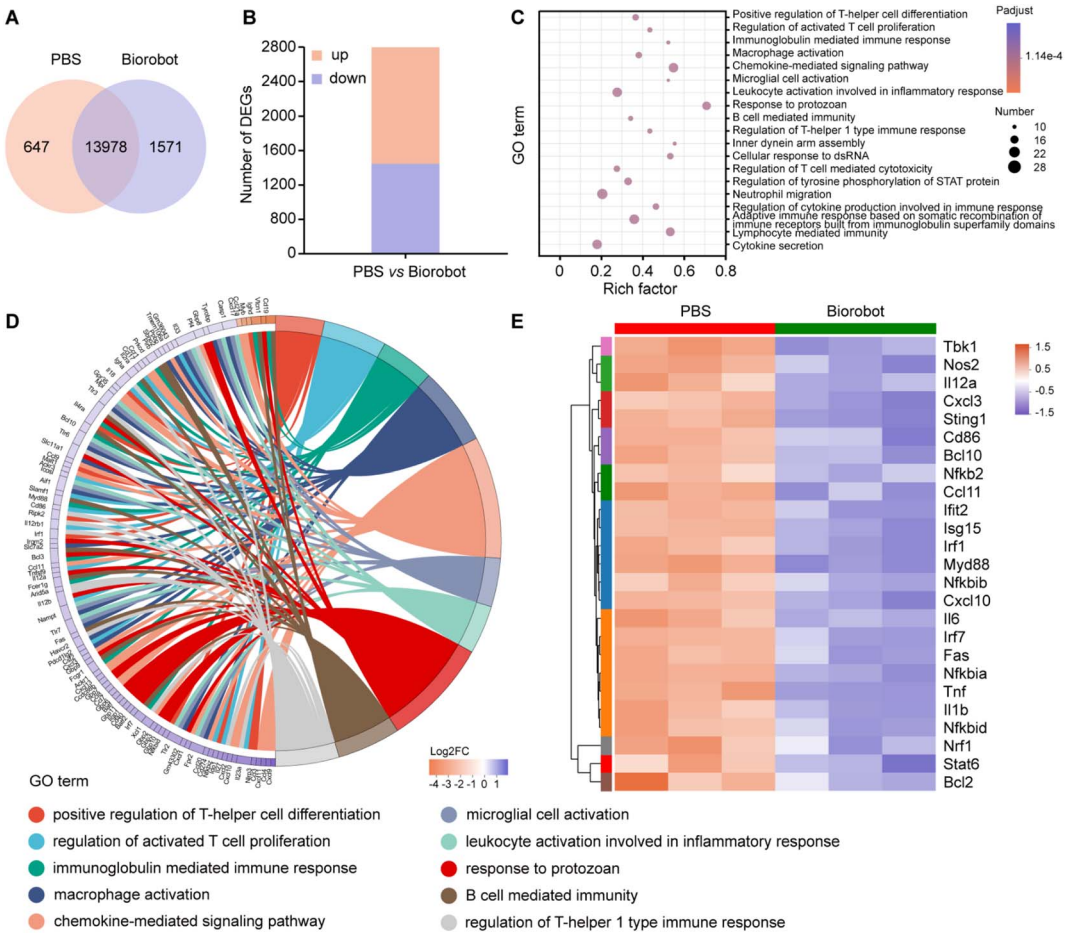

Fig. 8 Transcriptomic analysis of the treatment effects of Biorobot in pneumonia mice. (A) Venn diagram of expressed genes between PBS and Biorobot treatment in the lung tissues of pneumonia mice. (B) Differential gene expression after the treatment. (C) GO pathway enrichment analysis of the differentially expressed genes after the treatment. (D) GO enrichment chord diagram. (E) Heat map of downregulation of NF-κB and STING related genes after the treatment. The data are presented as mean ± s.d. ($n = 3$).

Next, we analyzed the gene expression data to identify differentially expressed genes related to the NF-κB and STING immune functions. NF-κB is a transcription factor that plays a key role in regulating the immune response to infections, while STING is an intracellular signaling protein that is involved in the detection of viral infections and the activation of the immune response. As shown in Fig. 8E, Biorobot treatment could induce differential expression of genes associated with immune function in lung tissues. The results are presented in the form of a heat map, which is a visual representation of data that uses color-coded cells to display values. In specific, Biorobot downregulated NF-κB and STING-related genes in lung tissues, suggesting that the simultaneous inhibition of multiple cytokine signaling pathways holds great promise as a strategy for modulating the immune response in various disease states. Therefore, Biorobot, which was designed to block both the NF-κB and STING inflammatory pathways can lead to a reduction in cytokine storm syndromes and an overall anti-inflammatory effect, which can guide the development of novel therapeutic strategies to improve the outcomes of patients suffering from severe inflammatory conditions.

Conclusions

In summary, the novel neutrophil-based therapeutic system called Biorobot has been developed to calm cytokine storms by enhancing synergistic anti-inflammatory effects. This system consists of living neutrophils encapsulating mannose-decorated liposomes containing the dual inhibitors TPCA-1 and H-151 (M-Lip@TH). Biorobot can selectively accumulate and release M-Lip@TH at inflammatory sites, allowing the dual inhibitors to be effectively endocytosed by macrophages. As a result, both the NF-κB signaling pathway and the cGAS-STING pathway are simultaneously blocked, leading to the inhibition of the production of inflammatory factors. *In vivo* studies have shown that Biorobot exhibits excellent pneumonia targeting ability and can effectively suppress the production of inflammatory cytokines, thereby improving the survival of pneumonia-afflicted mice. This innovative therapeutic platform holds great potential for the treatment of pneumonia and cytokine storm-associated diseases. By utilizing the body's own immune cells and targeting multiple inflammatory pathways, Biorobot offers a promising approach to manage severe inflammatory conditions and improve patient outcomes.

Ethical statement

Animals. Male C57BL/6 mice were purchased from Hangzhou Medical College (Hangzhou, China). All animal research was performed in accordance with National Institute of Health Guidelines under the protocols, approved by the ethics committee at the Affiliated Drum Tower Hospital of Nanjing University Medical School (SYXK(Su)2019-0056).

Data availability

The data that support the findings of this study are available from the corresponding authors upon reasonable request.

Author contributions

Y. G. and A. Z. performed the experiments, analyzed the data and wrote the manuscript. K. C. assisted experiment performance and data processing. X. Z. assisted data and formula analysis. Y. X., S. W. and X. N. conceptualized the projected. X. N. revised the manuscript and supervised the project. All the authors have given approval to the final version of the manuscript.

Conflicts of interest

There are no conflicts to declare.

Acknowledgements

The works were supported by the National Key Research and Development Program of China (Grant no. 2019YFA0802800, Grant no. 2021YFF1000700, Grant no. 2018YFB1105400), the National Natural Science Foundation of China (Grant no. 21472090, Grant no. 32301148), the Natural Science Foundation of Jiangsu Province (Grant no. BK20180334), the Fundamental Research Funds for Central Universities Nanjing University, the Key Research and Development Program of Jiangsu Provincial Department of Science and Technology of China (no. BE2019002) and Jiangsu Funding Program for Excellent Postdoctoral Talent (20220ZB23, 2023ZB486).

Notes and references

1 C. Cilloniz, C. Dominedo and A. Torres, Multidrug Resistant Gram-Negative Bacteria in Community-Acquired Pneumonia, *Crit. Care*, 2019, **23**, 79.
2 L. J. Quinton, A. J. Walkey and J. P. Mizgerd, Integrative Physiology of Pneumonia, *Physiol. Rev.*, 2018, **98**, 1417–1464.
3 R. Mendez, R. Menendez, I. Amara-Elori, L. Feced, A. Piro, P. Ramirez, A. Sempere, A. Ortega, J. F. Bermejo-Martin and A. Torres, Lymphopenic community-acquired pneumonia is associated with a dysregulated immune response and increased severity and mortality, *J. Infect.*, 2019, **78**, 423–431.
4 E. J. Giamarellos-Bourboulis, M. G. Netea, N. Rovina, K. Akinosoglou, A. Antoniadou, N. Antonakos, G. Damoraki, T. Gkavogianni, M. E. Adami, P. Katsaounou, M. Ntaganou, M. Kyriakopoulou, G. Dimopoulos, I. Koutsodimitropoulos, D. Velissaris, P. Koufargyris, A. Karageorgos, K. Katrini, V. Lekakis, M. Lupse, A. Kotsaki, G. Renieris, D. Theodoulou, V. Panou, E. Koukaki, N. Koulouris, C. Gogos and A. Koutsoukou, Complex Immune Dysregulation in COVID-19 Patients with Severe Respiratory Failure, *Cell Host Microbe*, 2020, **27**, 992–1000.
5 M. Soy, G. Keser, P. Atagunduz, F. Tabak, I. Atagunduz and S. Kayhan, Cytokine storm in COVID-19: pathogenesis and overview of anti-inflammatory agents used in treatment, *Clin. Rheumatol.*, 2020, **39**, 2085–2094.

6 N. Mangalmurti and C. A. Hunter, Cytokine Storms: Understanding COVID-19, *Immunity*, 2020, **53**, 19–25.
7 E. Della-Torre, C. Campochiaro, G. Cavalli, G. De Luca, A. Napolitano, S. La Marca, N. Boffini, V. Da Prat, G. Di Terlizzi, M. Lanzillotta, P. Rovere Querini, A. Ruggeri, G. Landoni, M. Tresoldi, F. Ciceri, A. Zangrillo, F. De Cobelli, L. Dagna, S.-R. S. Group and S.-R. S. G. members, Interleukin-6 blockade with sarilumab in severe COVID-19 pneumonia with systemic hyperinflammation: an open-label cohort study, *Ann. Rheum. Dis.*, 2020, **79**, 1277–1285.
8 R. Q. Cron, R. Caricchio and W. W. Chatham, Calming the cytokine storm in COVID-19, *Nat. Med.*, 2021, **27**, 1674–1675.
9 F. Katia, D. P. Myriam, C. Ucciferri, A. Auricchio, M. Di Nicola, M. Marchioni, C. Eleonora, S. Emanuela, F. Cipollone and J. Vecchiet, Efficacy of canakinumab in mild or severe COVID-19 pneumonia, *Immun., Inflammation Dis.*, 2021, **9**, 399–405.
10 G. Cavalli, G. De Luca, C. Campochiaro, E. Della-Torre, M. Ripa, D. Canetti, C. Oltolini, B. Castiglioni, C. Tassan Din, N. Boffini, A. Tomelleri, N. Farina, A. Ruggeri, P. Rovere-Querini, G. Di Lucca, S. Martinenghi, R. Scotti, M. Tresoldi, F. Ciceri, G. Landoni, A. Zangrillo, P. Scarpellini and L. Dagna, Interleukin-1 blockade with high-dose anakinra in patients with COVID-19, acute respiratory distress syndrome, and hyperinflammation: a retrospective cohort study, *Lancet Rheumatol.*, 2020, **2**, e325–e331.
11 E. C. Somers, G. A. Eschenauer, J. P. Troost, J. L. Golob, T. N. Gandhi, L. Wang, N. Zhou, L. A. Petty, J. H. Baang, N. O. Dillman, D. Frame, K. S. Gregg, D. R. Kaul, J. Nagel, T. S. Patel, S. Zhou, A. S. Lauring, D. A. Hanauer, E. Martin, P. Sharma, C. M. Fung and J. M. Pogue, Tocilizumab for Treatment of Mechanically Ventilated Patients With COVID-19, *Clin. Infect. Dis.*, 2021, **73**, e445–e454.
12 C. Campochiaro, E. Della-Torre, G. Cavalli, G. De Luca, M. Ripa, N. Boffini, A. Tomelleri, E. Baldissera, P. Rovere-Querini, A. Ruggeri, G. Monti, F. De Cobelli, A. Zangrillo, M. Tresoldi, A. Castagna, L. Dagna and T.-R. S. Group, Efficacy and safety of tocilizumab in severe COVID-19 patients: a single-centre retrospective cohort study, *Eur. J. Intern. Med.*, 2020, **76**, 43–49.
13 P. Mehta, D. F. McAuley, M. Brown, E. Sanchez, R. S. Tattersall, J. J. Manson and U. K. Hlh, Across Speciality Collaboration, COVID-19: consider cytokine storm syndromes and immunosuppression, *Lancet*, 2020, **395**, 1033–1034.
14 C. Valencia-Sanchez and D. M. Wingerchuk, A fine balance: Immunosuppression and immunotherapy in a patient with multiple sclerosis and COVID-19, *Mult. Scler. Relat. Disord.*, 2020, **42**, 102182.
15 R. S. Wallis, A. O'Garra, A. Sher and A. Wack, Host-directed immunotherapy of viral and bacterial infections: past, present and future, *Nat. Rev. Immunol.*, 2023, **23**, 121–133.
16 R. A. Grant, L. Morales-Nebreda, N. S. Markov, S. Swaminathan, M. Querrey, E. R. Guzman, D. A. Abbott, H. K. Donnelly, A. Donayre, I. A. Goldberg, Z. M. Klug, N. Borkowski, Z. Lu, H. Kihshen, Y. Politanska, L. Sichizya, M. Kang, A. Shilatifard, C. Qi, J. W. Lomasney, A. C. Argento, J. M. Kruser, E. S. Malsin, C. O. Pickens, S. B. Smith, J. M. Walter, A. E. Pawlowski, D. Schneider, P. Nannapaneni, H. Abdala-Valencia, A. Bharat, C. J. Gottardi, G. R. S. Budinger, A. V. Misharin, B. D. Singer, R. G. Wunderink and N. S. S. Investigators, Circuits between infected macrophages and T cells in SARS-CoV-2 pneumonia, *Nature*, 2021, **590**, 635–641.
17 C. S. Curran, T. Bolig and P. Torabi-Parizi, Mechanisms and Targeted Therapies for Pseudomonas aeruginosa Lung Infection, *Am. J. Respir. Crit. Care Med.*, 2018, **197**, 708–727.
18 M. Dukhinova, E. Kokinos, P. Kuchur, A. Komissarov and A. Shtro, Macrophage-derived cytokines in pneumonia: Linking cellular immunology and genetics, *Cytokine Growth Factor Rev.*, 2021, **59**, 46–61.
19 O. Takeuchi and S. Akira, Pattern recognition receptors and inflammation, *Cell*, 2010, **140**, 805–820.
20 S. Kumaran Satyanarayanan, D. El Kebir, S. Soboh, S. Butenko, M. Sekheri, J. Saadi, N. Peled, S. Assi, A. Othman, S. Schif-Zuck, Y. Feuermann, D. Barkan, N. Sher, J. G. Filep and A. Ariel, IFN-beta is a macrophage-derived effector cytokine facilitating the resolution of bacterial inflammation, *Nat. Commun.*, 2019, **10**, 3471.
21 W. A. Andrade, A. Firon, T. Schmidt, V. Hornung, K. A. Fitzgerald, E. A. Kurt-Jones, P. Trieu-Cuot, D. T. Golenbock and P. A. Kaminski, Group B Streptococcus Degrades Cyclic-di-AMP to Modulate STING-Dependent Type I Interferon Production, *Cell Host Microbe*, 2016, **20**, 49–59.
22 J. M. Berthelot and F. Liote, COVID-19 as a STING disorder with delayed over-secretion of interferon-beta, *EBioMedicine*, 2020, **56**, 102801.
23 X. Fan, K. Wang, Q. Lu, Y. Lu and J. Sun, Cell-Based Drug Delivery Systems Participate in the Cancer Immunity Cycle for Improved Cancer Immunotherapy, *Small*, 2023, **19**, e2205166.
24 Z. Zhao, A. Ukidve, J. Kim and S. Mitragotri, Targeting Strategies for Tissue-Specific Drug Delivery, *Cell*, 2020, **181**, 151–167.
25 S. Suryaprakash, Y. H. Lao, H. Y. Cho, M. Li, H. Y. Ji, D. Shao, H. Hu, C. H. Quek, D. Huang, R. L. Mintz, J. R. Bago, S. D. Hingtgen, K. B. Lee and K. W. Leong, Engineered Mesenchymal Stem Cell/Nanomedicine Spheroid as an Active Drug Delivery Platform for Combinational Glioblastoma Therapy, *Nano Lett.*, 2019, **19**, 1701–1705.
26 F. Combes, E. Meyer and N. N. Sanders, Immune cells as tumor drug delivery vehicles, *J. Controlled Release*, 2020, **327**, 70–87.
27 J. Zheng, R. Qi, C. Dai, G. Li and M. Sang, Enzyme Catalysis Biomotor Engineering of Neutrophils for Nanodrug Delivery and Cell-Based Thrombolytic Therapy, *ACS Nano*, 2022, **16**, 2330–2344.
28 M. Wu, H. Zhang, C. Tie, C. Yan, Z. Deng, Q. Wan, X. Liu, F. Yan and H. Zheng, MR imaging tracking of inflammation-activatable engineered neutrophils for

targeted therapy of surgically treated glioma, *Nat. Commun.*, 2018, **9**, 4777.

29 L. Sun, J. E. Zhou, T. Luo, J. Wang, L. Kang, Y. Wang, S. Luo, Z. Wang, Z. Zhou, J. Zhu, J. Yu, L. Yu and Z. Yan, Nanoengineered Neutrophils as a Cellular Sonosensitizer for Visual Sonodynamic Therapy of Malignant Tumors, *Adv. Mater.*, 2022, **34**, e2109969.

30 J. Che, A. Najer, A. K. Blakney, P. F. McKay, M. Bellahcene, C. W. Winter, A. Sintou, J. Tang, T. J. Keane, M. D. Schneider, R. J. Shattock, S. Sattler and M. M. Stevens, Neutrophils Enable Local and Non-Invasive Liposome Delivery to Inflamed Skeletal Muscle and Ischemic Heart, *Adv. Mater.*, 2020, **32**, e2003598.

31 Y. Han, Y. Liu, X. Ma, A. Shen, Y. Liu, N. Weeranoppanant, H. Dong, Y. Li, T. Ren, L. Kuai, B. Li, M. An and Y. Li, Antibiotics armed neutrophils as a potential therapy for brain fungal infection caused by chemotherapy-induced neutropenia, *Biomaterials*, 2021, **274**, 120849.

32 P. Baral, B. D. Umans, L. Li, A. Wallrapp, M. Bist, T. Kirschbaum, Y. Wei, Y. Zhou, V. K. Kuchroo, P. R. Burkett, B. G. Yipp, S. D. Liberles and I. M. Chiu, Nociceptor sensory neurons suppress neutrophil and gammadelta T cell responses in bacterial lung infections and lethal pneumonia, *Nat. Med.*, 2018, **24**, 417–426.

33 J. Bordon, S. Aliberti, R. Fernandez-Botran, S. M. Uriarte, M. J. Rane, P. Duvvuri, P. Peyrani, L. C. Morlacchi, F. Blasi and J. A. Ramirez, Understanding the roles of cytokines and neutrophil activity and neutrophil apoptosis in the protective *versus* deleterious inflammatory response in pneumonia, *Int. J. Infect. Dis.*, 2013, **17**, e76–e83.

34 D. Chu, X. Dong, X. Shi, C. Zhang and Z. Wang, Neutrophil-Based Drug Delivery Systems, *Adv. Mater.*, 2018, **30**, e1706245.

35 M. Merad and J. C. Martin, Pathological inflammation in patients with COVID-19: a key role for monocytes and macrophages, *Nat. Rev. Immunol.*, 2020, **20**, 355–362.

36 B. Allard, A. Panariti and J. G. Martin, Alveolar Macrophages in the Resolution of Inflammation, Tissue Repair, and Tolerance to Infection, *Front. Immunol.*, 2018, **9**, 1777.

37 E. Mortaz, S. D. Alipoor, I. M. Adcock, S. Mumby and L. Koenderman, Update on Neutrophil Function in Severe Inflammation, *Front. Immunol.*, 2018, **9**, 2171.

38 A. Margraf, K. Ley and A. Zarbock, Neutrophil Recruitment: From Model Systems to Tissue-Specific Patterns, *Trends Immunol.*, 2019, **40**, 613–634.

39 B. Colom, J. V. Bodkin, M. Beyrau, A. Woodfin, C. Ody, C. Rourke, T. Chavakis, K. Brohi, B. A. Imhof and S. Nourshargh, Leukotriene B4-Neutrophil Elastase Axis Drives Neutrophil Reverse Transendothelial Cell Migration In Vivo, *Immunity*, 2015, **42**, 1075–1086.

40 N. Germic, Z. Frangez, S. Yousefi and H. U. Simon, Regulation of the innate immune system by autophagy: monocytes, macrophages, dendritic cells and antigen presentation, *Cell Death Differ.*, 2019, **26**, 715–727.

41 T. H. Mogensen, Pathogen recognition and inflammatory signaling in innate immune defenses, *Clin. Microbiol. Rev.*, 2009, **22**, 240–273.

42 S. L. Doyle and L. A. O'Neill, Toll-like receptors: from the discovery of NFkappaB to new insights into transcriptional regulations in innate immunity, *Biochem. Pharmacol.*, 2006, **72**, 1102–1113.

43 Q. Chen, L. Sun and Z. J. Chen, Regulation and function of the cGAS-STING pathway of cytosolic DNA sensing, *Nat. Immunol.*, 2016, **17**, 1142–1149.

44 P. L. Podolin, J. F. Callahan, B. J. Bolognese, Y. H. Li, K. Carlson, T. G. Davis, G. W. Mellor, C. Evans and A. K. Roshak, Attenuation of murine collagen-induced arthritis by a novel, potent, selective small molecule inhibitor of IkappaB Kinase 2, TPCA-1 (2-[(aminocarbonyl) amino]-5-(4-fluorophenyl)-3-thiophenecarboxamide), occurs *via* reduction of proinflammatory cytokines and antigen-induced T cell Proliferation, *J. Pharmacol. Exp. Ther.*, 2005, **312**, 373–381.

45 S. M. Haag, M. F. Gulen, L. Reymond, A. Gibelin, L. Abrami, A. Decout, M. Heymann, F. G. van der Goot, G. Turcatti, R. Behrendt and A. Ablasser, Targeting STING with covalent small-molecule inhibitors, *Nature*, 2018, **559**, 269–273.

46 S. Benmerzoug, S. Rose, B. Bounab, D. Gosset, L. Duneau, P. Chenuet, L. Mollet, M. Le Bert, C. Lambers, S. Geleff, M. Roth, L. Fauconnier, D. Sedda, C. Carvalho, O. Perche, D. Laurenceau, B. Ryffel, L. Apetoh, A. Kiziltunc, H. Uslu, F. S. Albez, M. Akgun, D. Togbe and V. F. J. Quesniaux, STING-dependent sensing of self-DNA drives silica-induced lung inflammation, *Nat. Commun.*, 2018, **9**, 5226.

47 Q. Ma, Q. Fan, J. Xu, J. Bai, X. Han, Z. Dong, X. Zhou, Z. Liu, Z. Gu and C. Wang, Calming Cytokine Storm in Pneumonia by Targeted Delivery of TPCA-1 Using Platelet-Derived Extracellular Vesicles, *Matter*, 2020, **3**, 287–301.